NANO LETTERS
Letter
Cite This: Nano Lett. 2019, 19, 4355−4361
pubs.acs.org/NanoLett

Low Resistivity and High Breakdown Current Density of 10 nm Diameter van der Waals $TaSe_3$ Nanowires by Chemical Vapor Deposition

Thomas A. Empante,[†] Aimee Martinez,[†] Michelle Wurch,[†] Yanbing Zhu,[‡] Adane K. Geremew,[§] Koichi Yamaguchi,[†] Miguel Isarraraz,[†] Sergey Rumyantsev,[§,∥] Evan J. Reed,[‡] Alexander A. Balandin,[§] and Ludwig Bartels*,[†]

[†]Department of Chemistry and Material Science & Engineering Program, University of California—Riverside, Riverside, California 92521, United States

[‡]Department of Materials Science and Engineering, Stanford University, Stanford, California 94304, United States

[§]Nano-Device Laboratory, Department of Electrical and Computer Engineering, University of California, Riverside, California 92521, United States

[∥]Center for Terahertz Research and Applications, Institute of High Pressure Physics, Polish Academy of Sciences, Warsaw 01-142, Poland

Supporting Information

ABSTRACT: Micron-scale single-crystal nanowires of metallic $TaSe_3$, a material that forms $-Ta-Se_3-Ta-Se_3-$ stacks separated from one another by a tubular van der Waals (vdW) gap, have been synthesized using chemical vapor deposition (CVD) on a SiO_2/Si substrate, in a process compatible with semiconductor industry requirements. Their electrical resistivity was found unaffected by downscaling from the bulk to as little as 7 nm in nanowire width and height, in striking contrast to the resistivity of copper for the same dimensions. While the bulk resistivity of $TaSe_3$ is substantially higher than that of bulk copper, at the nanometer scale the $TaSe_3$ wires become competitive to similar-sized copper ones. Moreover, we find that the vdW $TaSe_3$ nanowires sustain current densities in excess of 10^8 A/cm^2 and feature an electromigration energy barrier twice that of copper. The results highlight the promise of quasi-one-dimensional transition metal trichalcogenides for electronic interconnect applications and the potential of van der Waals materials for downscaled electronics.

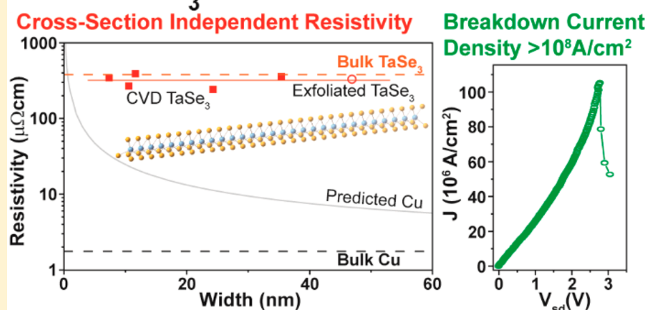

KEYWORDS: *transition metal trichalcogenides, nanowires, van der Waals materials, one-dimensional materials, interconnects, conductivity scaling*

The preparation, characterization, and application of two-dimensional (2D) materials such as graphene,[1−4] transition metal dichalcogenides (TMDs),[5−10] and MXenes[11−14] have attracted broad attention over the past years. This is partly due to the unique properties such materials exhibit when thinned to a single layer, yet it is also due to the astounding chemical stability and well-defined optical and electronic properties that these materials retain, even when only a single layer thin. Arguably, the latter is their most outstanding feature; it is caused by the presence of a planar van der Waals (vdW) gap in the crystallographic structure that affords some independence between the layers even in the bulk. When thinned to a single layer, the vdW gap prevents dangling bonds on the basal plane reducing scattering in transport and chemical reactivity to the environment. Recently, some of us have discovered almost 500 known compounds that resemble these 2D materials inasmuch as that their bulk contains vdW gaps, but these gaps are tubular in nature creating one-dimensional (1D) stacks of bound atoms separated from the neighboring stack similar to how a graphene or MoS_2 sheet is separated from the one above and below. Initial transport measurements on metallic 1D vdW tantalum triselenide ($TaSe_3$)[15−17] and zirconium tritelluride ($ZrTe_3$)[18] by some of us revealed good conductivity and exceptionally high breakdown current on mesoscopic exfoliated wire bundles; however, no systematic study of the dependence of the wire conductivity on its width/height has been conducted so far. Here we show that chemical vapor

Received: March 6, 2019
Revised: June 1, 2019
Published: June 18, 2019

Downloaded via UNIV OF CALIFORNIA RIVERSIDE on July 22, 2019 at 22:00:12 (UTC).
See https://pubs.acs.org/sharingguidelines for options on how to legitimately share published articles.

ACS Publications © 2019 American Chemical Society

DOI: 10.1021/acs.nanolett.9b00958
Nano Lett. 2019, 19, 4355−4361

deposition (CVD) allows the fabrication of wire bundles as small as a few nanometers across (i.e., consisting of a hundred atom stacks or less in parallel), scaled to the demand of the semiconductor industry for upcoming processing nodes. Most importantly, we find that such nanoscale bundles retain the bulk conductivity, much different to conventional metals, which at the 10 nm cross section scale are strongly affected by surface and grain-boundary scattering.[19−21] Additionally, we find that $TaSe_3$ exhibits a barrier to electromigration more than twice that of copper and can sustain current densities in excess of 10^8 A/cm^2. The favorable scaling of the conductivity with wire cross section renders these material of great interest as next generation interconnect material as copper reaches its scaling limits in 2023 according to the ITRS roadmap.[22−25]

This Letter focuses on the preparation and characterization of a specific transition metal trichalcogenide (TMT), $TaSe_3$, on a commercial 300 nm SiO_2/Si substrate using process parameters (ambient pressure, ≤400 °C process temperature, ≤5 min process duration) that are amenable to conventional back-end-of-line (BEOL) process limits. Despite the large interest in TMDs, TMTs have been largely left unstudied at the nanoscale; they have varying structures from 2D thin films to 1D wires and properties ranging from insulating to metallic.[17,26−28] $TaSe_3$ has a monoclinic unit cell and consists of stacks of Ta atoms, each of which are bonded to three selenium atoms above and below along the *b* axis (Figure 1a).

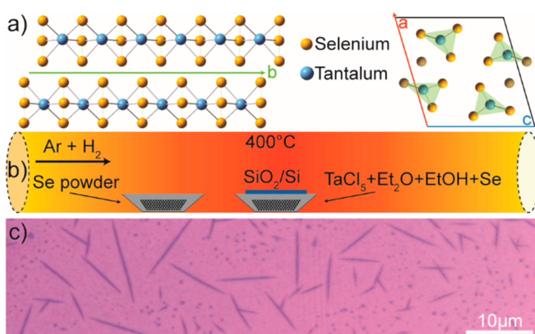

Figure 1. (a) Crystallographic structure of $TaSe_3$ consisting of four nanowire Ta−Se_3 stacks per unit cell along the *b* axis. The greyed atoms inside the unit cell correspond to those shown outside of it in order to highlight the selenium triangles between each tantalum plane. (b) Schematic representation of the chemical vapor deposition process inside a tube furnace. (c) Optical image of a population of $TaSe_3$ nanowires.

Neighboring −Ta−Se_3−Ta−Se_3− stacks are separated from one another by a tubular vdW gap exposing chalcogen atoms only, similar to the gap between the Se−Mo−Se layers in 2D $MoSe_2$. $TaSe_3$ has been known for a long time, and bulk samples have been prepared using chemical vapor transport (CVT), a process that requires long process times and is not amenable to current semiconductor processing paradigms; exfoliation of such samples yielded the results reported by some of us earlier.[15−17]

Interconnect performance is crucial for low-power high-clock-frequency computing: the transition from aluminum to copper interconnects starting some 20 years ago was driven by both the better conductivity of copper and the better manageability of electromigration in copper, the key failure mechanism for interconnects.[29,30] However, as the cross section of an interconnect becomes shorter than the electron mean free path (∼40 nm in copper),[19−21] its resistivity increases dramatically due to scattering at the material surface and at internal grain boundaries. A 1D material without surface dangling bonds or internal grain boundaries would, in theory, lack these drawbacks and be a prime candidate.

The best aspect ratio of interconnect cross sections has been studied intensely optimizing interconnect topology while reducing capacitive cross coupling. Modern processors use aspect ratios between 1.2 and 1.5 on the first four (0−3) metal layers.[31] We show a CVD method that natively generates nanoscale wires with a width to height aspect ratio of ∼1, close to the optimal one.

The 1D vdW $TaSe_3$ nanowire bundles are synthesized in a chemical vapor deposition (CVD) process using $TaCl_5$ and Se powder as reactants (both 99.99%, Sigma-Aldrich). Concurrent volatilization of both reactants under growth conditions is tantamount to sufficient chemical potential of each reactant on the surface during nanowire formation and elongation to the desired length. Thus, in order to match the vapor pressure of the tantalum precursor to that of selenium and the optimal growth temperature of $TaSe_3$, we first add diethyl ether to $TaCl_5$ in an inert nitrogen atmosphere to form the well-known metal chloride adduct $TaCl_5[OEt_2]$.[32] The adduct is dissolved in ethanol, leading possibly to (partial) ligand exchange; a small amount of gas evolution is observed when adding the ethanol. The Supporting Information provides more details on these adducts. Elemental selenium powder suspended in selenium-saturated ethanol is added, and the reactants are well mixed and dried in an alumina crucible. The Supporting Information shows micrographs that confirm the absence of nanowire formation at this stage. A 300 nm SiO_2/Si wafer substrate is placed across the alumina crucible, which is centered in a quartz process tube. A second crucible with elemental selenium is placed upstream so as to maintain selenium pressure during the entire growth process (Figure 1b). The process tube is placed in a tube furnace; a mixture of argon and hydrogen is used as ambient-pressure process gases. The furnace is heated to 400 °C as fast as possible (∼15 min), held for a few minutes (see below), and then rapidly cooled to ambient temperatures resulting in populations of $TaSe_3$ nanowires as shown in Figure 1c.

Raman spectroscopy (Horiba Labram HR800, 532 nm wavelength laser, linear polarization, 0.8 mW of laser power on sample) was used to characterize the nanowire bundles grown at hold times varying from 1 to 5 min (Figure 2a) at 400 °C. The feature at ∼180 cm^{-1} is typically referred to as B_2 or B_2/A_g in the literature. In addition, if we align the plane of polarization of the Raman excitation perpendicular to the nanowires, we find a second, weaker mode at ∼215 cm^{-1}. This peak in the literature is referred to as another A_{1g} mode. Computational modeling of the phonon spectrum and the associate atom displacement suggest that the dominant mode in Figure 2a is associated with axial wagging of the selenium trimer with regards to the Ta atom and the peak at ∼215 cm^{-1} with the symmetric and asymmetric stretch motion of the Se atoms in the trimer. The Supporting Information provides angle-dependent Raman spectra and graphic representations of the modes. While nanorods were formed in each instance, up to ∼3 min hold produced the nanowires with the sharpest Raman signature at ∼180 cm^{-1}; longer hold is associated with a broadening of the Raman mode by a higher energy shoulder. Supporting Information shows a table of the fit parameters of the spectra. Determining the average length of a large set of

DOI: 10.1021/acs.nanolett.9b00958
Nano Lett. 2019, 19, 4355−4361

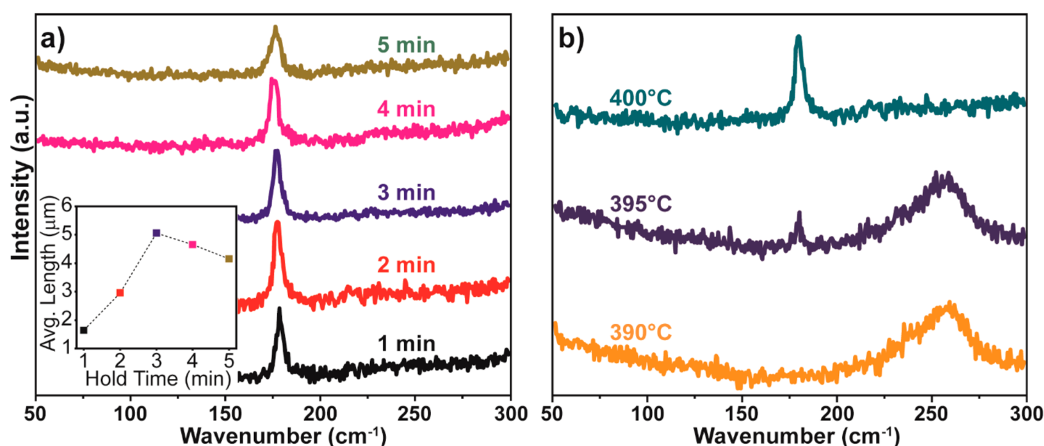

Figure 2. (a) Raman spectra of $TaSe_3$ nanowire bundles held for different duration at the growth temperature of 400 °C. A hold time beyond 3 min causes the Raman spectrum to broaden. The inset shows the resulting length distribution peaking at 3 min hold time. (b) Nanowire Raman spectra as a function of growth temperature. Starting at 400 °C, the desired peak at ~180 cm^{-1} is dominant.

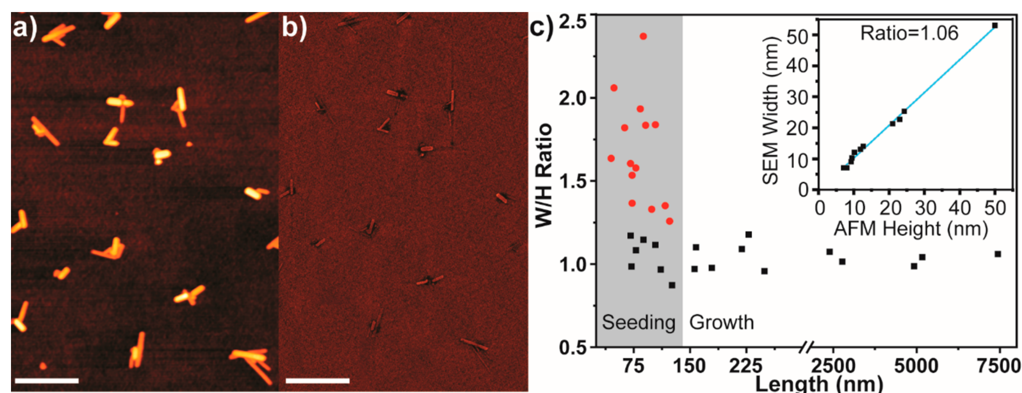

Figure 3. (a,b) Atomic force microscopy (AFM) and scanning electron microscopy (SEM) images, respectively, of the same population of $TaSe_3$ 1D vdW nanowire bundles (scale bar is 500 nm). (c) Width to height ratio of the 1D vdW $TaSe_3$ nanowires at seeding (gray area) and as uniaxial growth continues: longer wires have a width-to-height aspect ratio of practical unity. The inset plots SEM width vs the AFM height of the wires indicated by black markers in the main panel.

nanowires generated at each hold time using optical microscopy, we find a maximum wire length at ~3 min hold time (inset in Figure 2a). The Supporting Information shows histograms. This finding suggests that during the hold time the nanowires do not only form and elongate, but also can decompose, presumably from selenium loss. We studied the Raman spectra of the nanowires as a function of the peak process temperature (Figure 2b) and find that 400 °C is the minimum temperature at which nanowires with the desired Raman signature form. The nanowires with the broad spectral feature at ~260 cm^{-1} formed at process temperatures below 400 °C exhibit transport properties far inferior to those nanowires described in the remainder of this Letter; their precise composition is unknown to us.

In order to be of technological relevance, the $TaSe_3$ 1D vdW nanowires need to be prepared on the scale of a few nanometers in cross section yet significant in length. To this end we evaluated the length to width to height ratios in a population of nanowires. Figure 3a,b shows atomic force and scanning electron microscopy (AFM and SEM, respectively) images of the same population of growth seeds and short wires. We obtain the nanowire height from atomic force microscopy yet we use SEM to establish the nanowire width because of the finite size of any AFM tip and associated convolution of tip radius and nanowire width. Figure 3c shows the width-to-height aspect ratio of the nanowires plotted as a function of the nanowire length. Nanowires shorter in length than ~120 nm exhibit ratios between 0.75 and 2.5, which we attribute to the seeding of the growth (gray area). Longer nanowires have an aspect ratio very close to unity: as the axial growth sets in, the nanowires appear to minimize surface area by maintaining a width to height ratio near unity (black markers). Figure 3c includes also a significant number of long nanowires that form the basis of the transport measurements in the next section of this Letter. The inset shows the dependence of width to height for the black markers of the main panel. The slope is 1.06.

For measurement of the electrical transport properties of the $TaSe_3$ nanowires we employed electron beam lithography (EBL) to fabricate contacts consisting of 5 nm of yttrium for adhesion and 50 nm of gold for conduction and stability. Previous studies of $TaSe_3$ nanowires[15−17] used encapsulation in *h*-BN to avoid surface decomposition by oxygen and moisture from the air. Striving to utilize only scalable methods in our work, we took a different approach: immediately following removal from the process tube, we cap the substrate containing the 1D vdW $TaSe_3$ nanowires with spin-coated poly(methyl methacrylate) (C5 PMMA) resist under a nitrogen-atmosphere. Subsequently, we characterize the nanowires by Raman spectroscopy through the PMMA film and then use the same resist film to fabricate electrical contacts.

DOI: 10.1021/acs.nanolett.9b00958
Nano Lett. 2019, 19, 4355−4361

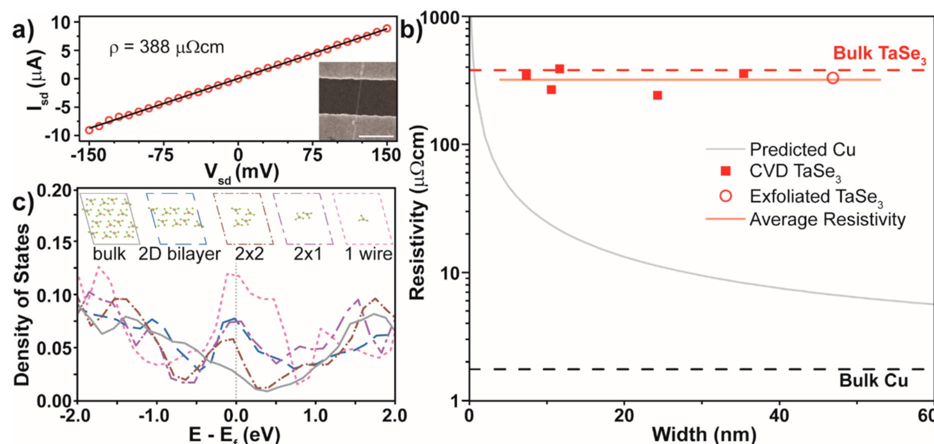

Figure 4. (a) Source-drain current vs voltage (I_{sd} vs V_{sd}) for a 11.6 nm $TaSe_3$ nanowire; a linear dependence is observed in this two-probe measurement that corresponds to the current density shown on the *y*-axis and the resistivity highlighted. The inset shows an SEM image of a 1D vdW $TaSe_3$ nanowire bridging two electrodes (scale bar is 500 nm). (b) Resistivity of $TaSe_3$ nanowire bundles with width-to-height aspect ratios near unity (1.0−1.1) as a function of bundle width. For reference, we include bulk values for copper and $TaSe_3$ as dashed lines, as well as a prediction for the scaling of the copper resistivity with wire width based on ref 21. The smallest exfoliated nanowire of our prior studies is indicated as an open dot.[15−17] (c) calculated density of states (DOS) near the Fermi level (E_F) for bulk $TaSe_3$, a 2D bilayer of wires, a 2 × 2 wire bundle, a 2 × 1 wire bundle, and a single wire. The confined wire geometries have higher DOS at E_F than the bulk material, suggesting that quantum confinement does not adversely affect charge transport in $TaSe_3$.

Care is taken to minimize the time between development and metal deposition so as to reduce air exposure of the sample. Immediately following metal liftoff, we again spin coat the sample with a layer of PMMA in a nitrogen glovebox. Subsequently, a second EBL process is performed to remove resist from the surface of the probe pads only. Electrical characterization proceeds in a nitrogen atmosphere.

Figure 4a shows a typical current−voltage (*I*−*V*) diagram measured on a $TaSe_3$ nanowire with width and height of ∼11.6 nm each. We use electrodes separated by 500 nm (inset). A linear *I*−*V* dependence is observed, from which a resistivity ρ of 388 $\mu\Omega$ cm is obtained.

We tested a large number of nanowires, each time followed by AFM and SEM characterization of their respective width and height. Figure 4b shows the resistivity of wires with width ≤50 nm and cross section aspect ratios near unity (1.0−1.1). In a few cases we found wires that exhibited significant nonlinear response for small voltage, which we ascribe to contact resistance. These were omitted from Figure 4b. The figure reveals that the specific resistance of 1D vdW $TasSe_3$ nanowires is independent of the cross section of the wire bundle down to 7 nm in width and height. This presents a marked contrast to the behavior of copper at the nanoscale for which Figure 4b includes a reference line based on the work of Steinhogel et al.[21] assuming surface *p* and grain boundary *R* scattering amplitudes of 0.5 and 0.6, respectively. At a few nanometer wire widths, the resistivity of $TaSe_3$ becomes competitive to that of copper, assuming that a pinhole-free deposition of copper wires is possible at that width scale, which is not immediately apparent.[33]

If scattering does not limit the scaling of the conductivity of $TaSe_3$ nanowires, we explore whether quantum confinement perpendicular to the nanowire direction may do so. To this end, we assume that the conductivity of a metallic material in first order scales with its density of state (DOS) near the Fermi level (E_F) and calculate the DOS of various nanowire bundle configurations. We employ density functional theory as implemented in the Vienna Ab initio Simulation Package (VASP)[34] using the projector augmented wave method[35,36] and treating the electron exchange-correlation interaction by the generalized gradient approximation (GGA) functional of Perdew, Burke, and Ernzerhof (PBE).[37] All calculations use periodic boundary conditions, and the Brillouin zone was sampled by a 2 × 7 × 2 Monkhorst−Pack k-point grid.[38]

Figure 4c compares the density of states (DOS) of an infinite bulk of $TaSe_3$ (solid line) to an infinite 2D bilayer of wires, bundles of 2 × 2 and 2 × 1 wires, as well as a single wire. In each case we find considerable DOS near the Fermi level (E_F) and no band gap. Indeed, as the wire bundle is thinned to a bilayer and a finite number of wire stacks, the DOS near E_F increases. This finding suggests that—at least for some wire bundle geometries—a higher native conductivity is possible than for the bulk case. We recognize, however, that this analysis omits fundamental stability limitations (such as the Mermin−Wagner theorem[39]) yet we note that additional research is necessary to fathom their impact as shown for graphene.[40] The smallest wire bundle for which we obtained transport measurements had a width and height of ∼7 nm (Figure 4b) and thus as few as ∼10 × 10 wires in parallel; it is almost an order of magnitude larger than the computationally readily tractable ones of Figure 4c.

Finally, we turn to the stability of the 1D vdW nanowires with regards to degradation under transport. Measurements of the low-frequency noise are commonly used to assess the quality and reliability of conventional[41−45] and novel 2D materials[16,18,46] for device applications. Changes in the noise spectra can serve as a convenient indicator of the onset of electromigration and other material degradation mechanisms. In the context of interconnect research, the low-frequency noise can provide a fast estimate of the device's mean time to failure. The low-frequency noise measurements were performed using an experimental setup consisting of a "quiet" battery, a potentiometer biasing circuit, a low noise amplifier, and a spectrum analyzer; additional details have been reported elsewhere.[47,48]

Figure 5a shows the normalized current noise spectral density S_I/I^2 as a function of frequency *f* for a $TaSe_3$ nanowire with a cross-section of ∼10 × 10 nm^2. The noise level S_I/I^2 of

DOI: 10.1021/acs.nanolett.9b00958
Nano Lett. 2019, 19, 4355−4361

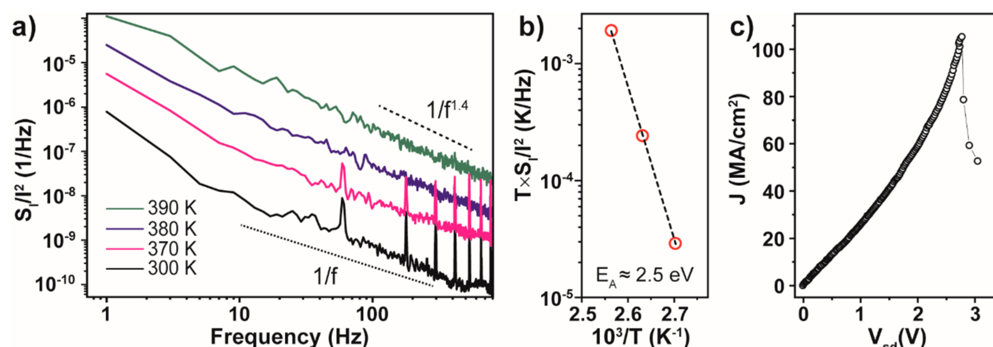

Figure 5. (a) Normalized current noise spectral density of a ∼10 × 10 nm^2 (width × height) CVD 1D vdW $TaSe_3$ nanowire bundle at different temperatures T using a source-drain voltage V_{sd} of 0.1 V. (b) Arrhenius plot of $T \times S_I/I^2$ vs 1000/T for a frequency f of 11 Hz. The extracted activation energy E_A is 2.57 eV. (c) Current density J response of a ∼ 7 × 7 nm^2 nanowire as the voltage is slowly increased. Failure occurs at a current density in excess of 10^8 A/cm^2.

∼10^{-8} Hz^{-1} at f = 10 Hz and T = 300 K in the downscaled CVD $TaSe_3$ nanowires is appreciably low. Although it is higher than measured in conventional metals[49,50] and also for larger cross section exfoliated $TaSe_3$ nanowires,[16,50] the latter is expected because the noise originating from a volume of independent fluctuators scales inversely proportional to the size of the volume.[41] Indeed, one can write for the noise spectral density[41−43] $S_I/I^2 = \alpha_H/Nf$, where α_H is the coefficient of proportionality referred to as the Hooge parameter, and $N = nV$, where n is the concentration of the charge carriers and V is the volume of the sample. The noise levels of 10^{-9}−10^{-5} Hz^{-1} are found in conventional transistors and other electronic devices.[43]

Figure 5a reveals increase in the noise level with increasing temperature. The informative frequency range from 10 to ∼400 Hz exhibits a deviation from pure 1/f noise; approximately 1/$f^{1.4}$ provides the best fit at elevated temperatures. This trend is consistent with observations on thicker exfoliated $TaSe_3$ nanowires.[16] In metals, the deviation from 1/f-type behavior is commonly attributed to the onset of electromigration. We construct an Arrhenius plot of TS_I/I^2 vs 1000/T (Figure 5b) to extract the activation energy (E_A) for the noise inducing process in CVD 1D vdW $TaSe_3$ nanowires. The resultant value of ∼2.5 eV is larger than that for exfoliated $TaSe_3$ nanowires[16] and more than twice that for electromigration in copper (0.76−1.10 eV) and aluminum (0.67- 1.14 eV) using similar measurements.[44,45,50,51] This finding suggests very good resistance of CVD $TaSe_3$ 1D vdW nanowire to electromigration.

The electromigration resilience of the CVD 1D vdW $TaSe_3$ nanowires is confirmed by successively increasing the voltage applied to a 7 × 7 nm^2 wire bundle (about 100 parallel Ta−Se_3 stacks in total). Figure 5c shows that the wire bundle was able to sustain in excess of 10^8 A/cm^2 before electrical breakdown. This current density is an order of magnitude higher than that found for thicker, exfoliated $TaSe_3$, and also slightly better than our previous findings for $ZrTe_3$.[18] We note that acquiring the data set of Figure 5c took almost an hour of slowly increasing the bias, so that self-heating may have contributed to reduced overall current carrying capacity and increased susceptibility to electromigration. Embedding the nanowire with a better thermal sink than the underlying SiO_2 substrate and the surrounding PMMA resist may result in even higher sustained current densities.

In conclusion, we find that chemical vapor deposition allows the growth of $TaSe_3$ nanowires on a SiO_2 substrate that are competitive in resistivity to conventional metals scaled to sub-10-nanometer wire diameters, while offering significantly enhanced electromigration resilience and breakdown current. The growth proceeds at back-end-of-line compatible temperatures (∼400 °C) and because it takes just a few minutes, it has a comparatively low thermal budget impact. Future work will adapt prior findings on the spatially selective growth of TMD materials[52−55] so as to generate the $TaSe_3$ nanowires not randomly dispersed on the sample but at desired locations only.

■ ASSOCIATED CONTENT

Supporting Information

The Supporting Information is available free of charge on the ACS Publications website at DOI: 10.1021/acs.nanolett.9b00958.

Electron microscopy imaging of the CVD precursors and $TaSe_3$ nanowires; thermal behavior of the resistance of $TaSe_3$ nanowires; angle-dependent Raman spectroscopy of nanowires; size distribution of nanowires (PDF)

■ AUTHOR INFORMATION

Corresponding Author

*E-mail: bartels@ucr.edu or ludwig.bartels@ucr.edu.

ORCID

Thomas A. Empante: 0000-0003-0636-385X
Adane K. Geremew: 0000-0001-6171-7265
Ludwig Bartels: 0000-0002-3964-4538

Notes

The authors declare no competing financial interest.

■ ACKNOWLEDGMENTS

This project was supported by the Semiconductor Research Corporation (SRC) under contract 2018-NM-2796. The noise measurements and the computational work were supported, in part, by the National Science Foundation (NSF) under grants EFRI-1433395 and DMR-1455050, respectively. Ancillary support originated form the US Air Force Office of Scientific Research under Grant FA9550-14-1-0378.

■ REFERENCES

(1) Novoselov, K. S.; Geim, A. K.; Morozov, S. V.; Jiang, D.; Zhang, Y.; Dubonos, S. V.; Grigorieva, I. V.; Firsov, A. A. Electric field effect in atomically thin carbon films. *Science* **2004**, *306* (5696), 666−669.

DOI: 10.1021/acs.nanolett.9b00958
Nano Lett. 2019, 19, 4355−4361

(2) Castro Neto, A. H.; Guinea, F.; Peres, N. M. R.; Novoselov, K. S.; Geim, A. K. The electronic properties of graphene. *Rev. Mod. Phys.* **2009**, *81* (1), 109.
(3) Lee, C.; Wei, X. D.; Kysar, J. W.; Hone, J. Measurement of the elastic properties and intrinsic strength of monolayer graphene. *Science* **2008**, *321* (5887), 385−388.
(4) Zhang, Y. B.; Tan, Y. W.; Stormer, H. L.; Kim, P. Experimental observation of the quantum Hall effect and Berry's phase in graphene. *Nature* **2005**, *438* (7065), 201−204.
(5) Chhowalla, M.; Shin, H. S.; Eda, G.; Li, L. J.; Loh, K. P.; Zhang, H. The chemistry of two-dimensional layered transition metal dichalcogenide nanosheets. *Nat. Chem.* **2013**, *5* (4), 263−75.
(6) Bernardi, M.; Palummo, M.; Grossman, J. C. Extraordinary Sunlight Absorption and One Nanometer Thick Photovoltaics Using Two-Dimensional Monolayer Materials. *Nano Lett.* **2013**, *13* (8), 3664−3670.
(7) Bhimanapati, G. R.; Lin, Z.; Meunier, V.; Jung, Y.; Cha, J.; Das, S.; Xiao, D.; Son, Y.; Strano, M. S.; Cooper, V. R.; Liang, L. B.; Louie, S. G.; Ringe, E.; Zhou, W.; Kim, S. S.; Naik, R. R.; Sumpter, B. G.; Terrones, H.; Xia, F. N.; Wang, Y. L.; Zhu, J.; Akinwande, D.; Alem, N.; Schuller, J. A.; Schaak, R. E.; Terrones, M.; Robinson, J. A. Recent Advances in Two-Dimensional Materials beyond Graphene. *ACS Nano* **2015**, *9* (12), 11509−11539.
(8) Empante, T. A.; Zhou, Y.; Klee, V.; Nguyen, A. E.; Lu, I. H.; Valentin, M. D.; Naghibi Alvillar, S. A.; Preciado, E.; Berges, A. J.; Merida, C. S.; Gomez, M.; Bobek, S.; Isarraraz, M.; Reed, E. J.; Bartels, L. Chemical Vapor Deposition Growth of Few-Layer $MoTe_2$ in the 2H, 1T′, and 1T Phases: Tunable Properties of $MoTe_2$ Films. *ACS Nano* **2017**, *11*, 900.
(9) Mak, K. F.; Lee, C.; Hone, J.; Shan, J.; Heinz, T. F. Atomically thin MoS_2: a new direct-gap semiconductor. *Phys. Rev. Lett.* **2010**, *105* (13), 136805.
(10) Splendiani, A.; Sun, L.; Zhang, Y. B.; Li, T. S.; Kim, J.; Chim, C. Y.; Galli, G.; Wang, F. Emerging photoluminescence in monolayer MoS_2. *Nano Lett.* **2010**, *10* (4), 1271−1275.
(11) Lukatskaya, M. R.; Mashtalir, O.; Ren, C. E.; Dall'Agnese, Y.; Rozier, P.; Taberna, P. L.; Naguib, M.; Simon, P.; Barsoum, M. W.; Gogotsi, Y. Cation Intercalation and High Volumetric Capacitance of Two-Dimensional Titanium Carbide. *Science* **2013**, *341* (6153), 1502−1505.
(12) Naguib, M.; Mashtalir, O.; Carle, J.; Presser, V.; Lu, J.; Hultman, L.; Gogotsi, Y.; Barsoum, M. W. Two-Dimensional Transition Metal Carbides. *ACS Nano* **2012**, *6* (2), 1322−1331.
(13) Naguib, M.; Mochalin, V. N.; Barsoum, M. W.; Gogotsi, Y. 25th Anniversary Article: MXenes: A New Family of Two-Dimensional Materials. *Adv. Mater.* **2014**, *26* (7), 992−1005.
(14) Khazaei, M.; Arai, M.; Sasaki, T.; Chung, C. Y.; Venkataramanan, N. S.; Estili, M.; Sakka, Y.; Kawazoe, Y. Novel Electronic and Magnetic Properties of Two-Dimensional Transition Metal Carbides and Nitrides. *Adv. Funct. Mater.* **2013**, *23* (17), 2185−2192.
(15) Geremew, A.; Rumyantsev, S.; Bloodgood, M. A.; Salguero, T. T.; Balandin, A. A. Unique features of the generation−recombination noise in quasi-one-dimensional van der Waals nanoribbons. *Nanoscale* **2018**, *10*, 19749.
(16) Liu, G. X.; Rumyantsev, S.; Bloodgood, M. A.; Salguero, T. T.; Shur, M.; Balandin, A. A. Low-Frequency Electronic Noise in Quasi-1D TaSe3 van der Waals Nanowires. *Nano Lett.* **2017**, *17* (1), 377−383.
(17) Stolyarov, M. A.; Liu, G. X.; Bloodgood, M. A.; Aytan, E.; Jiang, C. L.; Samnakay, R.; Salguero, T. T.; Nika, D. L.; Rumyantsev, S. L.; Shur, M. S.; Bozhilov, K. N.; Balandin, A. A. Breakdown current density in h-BN-capped quasi-1D $TaSe_3$ metallic nanowires: prospects of interconnect applications. *Nanoscale* **2016**, *8* (34), 15774−15782.
(18) Geremew, A.; Bloodgood, M. A.; Aytan, E.; Woo, B. W. K.; Corber, S. R.; Liu, G.; Bozhilov, K.; Salguero, T. T.; Rumyantsev, S.; Rao, M. P.; Balandin, A. A. Current Carrying Capacity of Quasi-1D $ZrTe_3$ Van Der Waals Nanoribbons. *IEEE Electron Device Lett.* **2018**, *39* (5), 735−738.
(19) Gall, D. Electron mean free path in elemental metals. *J. Appl. Phys.* **2016**, *119* (8), 085101.
(20) Steinhogl, W.; Schindler, G.; Steinlesberger, G.; Traving, M.; Engelhardt, M. Comprehensive study of the resistivity of copper wires with lateral dimensions of 100 nm and smaller. *J. Appl. Phys.* **2005**, *97* (2), 023706.
(21) Steinhogl, W.; Schindler, G.; Steinlesberger, G.; Engelhardt, M. Size-dependent resistivity of metallic wires in the mesoscopic range. *Phys. Rev. B* **2002**, *66* (7), 075414.
(22) Li, B. Z.; Sullivan, T. D.; Lee, T. C.; Badami, D. Reliability challenges for copper interconnects. *Microelectron. Reliab.* **2004**, *44* (3), 365−380.
(23) Lloyd, J. R.; Clement, J. J. Electromigration damage due to copper depletion in Al/Cu alloy conductors. *Appl. Phys. Lett.* **1996**, *69* (17), 2486−2488.
(24) Hu, C. K.; Luther, B.; Kaufman, F. B.; Hummel, J.; Uzoh, C.; Pearson, D. J. Copper Interconnection Integration and Reliability. *Thin Solid Films* **1995**, *262* (1−2), 84−92.
(25) Kapur, P.; Chandra, G.; McVittie, J. P.; Saraswat, K. C. Technology and reliability constrained future copper interconnects - Part II: Performance implications. *IEEE Trans. Electron Devices* **2002**, *49* (4), 598−604.
(26) Bjerkelund, E.; Kjekshus, A. On the Properties of TaS_3, $TaSe_3$ and $TaTe_4$. *Z. Anorg. Allg. Chem.* **1964**, *328* (5−6), 235−242.
(27) Canadell, E.; Rachidi, I. E. I.; Pouget, J. P.; Gressier, P.; Meerschaut, A.; Rouxel, J.; Jung, D.; Evain, M.; Whangbo, M. H. Comparison of the Electronic-Structures of Layered Transition-Metal Trichalcogenides $TaSe_3$, TaS_3, and $NbSe_3$. *Inorg. Chem.* **1990**, *29* (7), 1401−1407.
(28) Ariya, S. M.; Zaslavskii, A. I.; Matveeva, I. I. Khimiya Soedinenii Peremennogo Sostava 0.4. Sistema Tantal-Selen. *Zhurnal Obshchei Khimii* **1956**, *26* (9), 2373−2375.
(29) Heidenreich, J.; Edelstein, D.; Goldblatt, R.; Cote, W.; Uzoh, C.; Lustig, N.; McDevitt, T.; Stamper, A.; Simon, A.; Dukovic, J.; Andricacos, P.; Wachnik, R.; Rathore, H.; Katsetos, T.; McLaughlin, P.; Luce, S.; Slattery, J.; Ieee, E. D. S. Copper dual damascene wiring for sub-0.25 mu m CMOS technology. *Proceedings of the Ieee 1998 International Interconnect Technology Conference* **1998**, 151−153.
(30) Bohr, M.; Ahmed, S. S.; Ahmed, S. U.; Bost, M.; Ghani, T.; Greason, J.; Hainsey, R.; Jan, C.; Packan, P.; Sivakumar, S.; Thompson, S.; Tsai, J.; Yang, S. IEEE, A high performance 0.25 mu m logic technology optimized for 1.8 V operation. *IEDM - International Electron Devices Meeting, Technical Digest 1996* 1996, 847−850.
(31) Fischer, K.; Agostinelli, M.; Allen, C.; Bahr, D.; Bost, M.; Charvat, P.; Chikarmane, V.; Fu, Q.; Ganpule, C.; Haran, M.; Heckscher, M.; Hiramatsu, H.; Hwang, E.; Jain, P.; Jin, I.; Kasim, R.; Kosaraju, S.; Lee, K. S.; Liu, H.; McFadden, R.; Nigam, S.; Patel, R.; Pelto, C.; Plekhanov, P.; Prince, M.; Puls, C.; Rajamani, S.; Rao, D.; Reese, P.; Rosenbaum, A.; Sivakumar, S.; Song, B.; Uncuer, M.; Williams, S.; Yang, M.; Yashar, P.; Natarajan, S. Low-k Interconnect Stack with multi-layer Air Gap and Tri-Metal-Insulator-Metal Capacitors for 14nm High Volume Manufacturing. *2015 IEEE International Interconnect Technology Conference and 2015 IEEE Materials for Advanced Metallization Conference*; IITC/MAM, 2015; pp 5−7.
(32) Marchetti, F.; Pampaloni, G. Interaction of niobium and tantalum pentahalides with O-donors: coordination chemistry and activation reactions. *Chem. Commun.* **2012**, *48* (5), 635−653.
(33) Wang, T. C.; Wang, Y. L.; Hsieh, T. E.; Chang, S. C.; Cheng, Y. L. Copper voids improvement for the copper dual damascene interconnection process. *J. Phys. Chem. Solids* **2008**, *69* (2−3), 566−571.
(34) Kresse, G.; Furthmüller, J. Efficiency of ab-initio total energy calculations for metals and semiconductors using a plane-wave basis set. *Comput. Mater. Sci.* **1996**, *6*, 15.
(35) Blochl, P. E. Projector Augmented-Wave Method. *Phys. Rev. B: Condens. Matter Mater. Phys.* **1994**, *50* (24), 17953−17979.

DOI: 10.1021/acs.nanolett.9b00958
Nano Lett. 2019, 19, 4355−4361

(36) Kresse, G.; Joubert, D. From ultrasoft pseudopotentials to the projector augmented-wave method. *Phys. Rev. B: Condens. Matter Mater. Phys.* **1999**, *59* (3), 1758−1775.
(37) Perdew, J. P.; Burke, K.; Ernzerhof, M. Generalized gradient approximation made simple. *Phys. Rev. Lett.* **1996**, *77* (18), 3865−3868.
(38) Monkhorst, H. J.; Pack, J. D. Special Points for Brillouin-Zone Integrations. *Phys. Rev. B* **1976**, *13* (12), 5188−5192.
(39) Mermin, N. D.; Wagner, H. Absence of Ferromagnetism or Antiferromagnetism in One- or 2-Dimensional Isotropic Heisenberg Models. *Phys. Rev. Lett.* **1966**, *17* (22), 1133.
(40) O'Hare, A.; Kusmartsev, F. V.; Kugel, K. I. A Stable "Flat" Form of Two-Dimensional Crystals: Could Graphene, Silicene, Germanene Be Minigap Semiconductors? *Nano Lett.* **2012**, *12* (2), 1045−1052.
(41) Dutta, P.; Horn, P. M. Low-Frequency Fluctuations in Solids - 1-F Noise. *Rev. Mod. Phys.* **1981**, *53* (3), 497−516.
(42) Vandamme, L. K. J. Noise as a Diagnostic-Tool for Quality and Reliability of Electronic Devices. *IEEE Trans. Electron Devices* **1994**, *41* (11), 2176−2187.
(43) Balandin, A. A. *Noise and Fluctuations Control in Electronic Devices*; American Scientific Publishers: Los Angeles, CA, 2002.
(44) Beyne, S.; Croes, K.; De Wolf, I.; Tokei, Z. 1/f noise measurements for faster evaluation of electromigration in advanced microelectronics interconnections. *J. Appl. Phys.* **2016**, *119* (18), 184302.
(45) Bagnoli, P. E.; Ciofi, C.; Neri, B.; Pennelli, G. Electromigration in Al based stripes: Low frequency noise measurements and MTF tests. *Microelectron. Reliab.* **1996**, *36* (7−8), 1045−1050.
(46) Balandin, A. A. Low-frequency 1/f noise in graphene devices. *Nat. Nanotechnol.* **2013**, *8* (8), 549−555.
(47) Rumyantsev, S.; Liu, G.; Stillman, W.; Shur, M.; Balandin, A. A. Electrical and noise characteristics of graphene field-effect transistors: ambient effects, noise sources and physical mechanisms. *J. Phys.: Condens. Matter* **2010**, *22* (39), 395302.
(48) Liu, G. X.; Rumyantsev, S.; Bloodgood, M. A.; Salguero, T. T.; Balandin, A. A. Low-Frequency Current Fluctuations and Sliding of the Charge Density Waves in Two-Dimensional Materials. *Nano Lett.* **2018**, *18* (6), 3630−3636.
(49) Dutta, P.; Dimon, P.; Horn, P. M. Energy Scales for Noise Processes in Metals. *Phys. Rev. Lett.* **1979**, *43* (9), 646−649.
(50) Koch, R. H.; Lloyd, J. R.; Cronin, J. 1/F Noise and Grain-Boundary Diffusion in Aluminum and Aluminum-Alloys. *Phys. Rev. Lett.* **1985**, *55* (22), 2487−2490.
(51) Chen, T. M.; Yassine, A. M. Electrical Noise and Vlsi Interconnect Reliability. *IEEE Trans. Electron Devices* **1994**, *41* (11), 2165−2172.
(52) Liao, I.; Barroso, D.; nguyen, A.; Duong, N.; Yurek, Q.; merida, C. S.; Pena, P.; Lu, I.-H.; valentin, M.; Stecklein, G.; Bartels, L. Hybrid Single-Layer/Bulk Tungsten Diselenide Transistors by Lithographic Encoding of Material Thickness in Chemical Vapor Deposition. *2D Mater.* **2019**, *6*, 015017.
(53) Sun, D. Z.; Nguyen, A. E.; Barroso, D.; Zhang, X.; Preciado, E.; Bobek, S.; Klee, V.; Mann, J.; Bartels, L. Chemical vapor deposition growth of a periodic array of single-layer MoS2 islands via lithographic patterning of an SiO2/Si substrate. *2D Mater.* **2015**, *2* (4), 045014.
(54) Gong, C. H.; Hu, K.; Wang, X. P.; Wangyang, P. H.; Yan, C. Y.; Chu, J. W.; Liao, M.; Dai, L. P.; Zhai, T. Y.; Wang, C.; Li, L.; Xiong, J. 2D Nanomaterial Arrays for Electronics and Optoelectronics. *Adv. Funct. Mater.* **2018**, *28* (16), 1706559.
(55) Young, J. R.; Chilcote, M.; Barone, M.; Xu, J. S.; Katoch, J.; Luo, Y. K.; Mueller, S.; Asel, T. J.; Fullerton-Shirey, S. K.; Kawakami, R.; Gupta, J. A.; Brillson, L. J.; Johnston-Halperin, E. Uniform large-area growth of nanotemplated high-quality monolayer MoS2. *Appl. Phys. Lett.* **2017**, *110* (26), 263103.

DOI: 10.1021/acs.nanolett.9b00958
Nano Lett. 2019, 19, 4355−4361